Published in final edited form as:
J Biophotonics. 2008 March ; 1(1): 24–35. doi:10.1002/jbio.200710010.

Biophysical Response to Pulsed Laser Microbeam-Induced Cell Lysis and Molecular Delivery

Amy N. Hellman[a,b,c], **Kaustubh R. Rau**[b,c,d], **Helen H. Yoon**[e], and **Vasan Venugopalan**[b,c]

[a]Dept. of Bioengineering, University of California, San Diego, La Jolla, CA USA 92093-0412

[b]Dept. of Chemical Engineering & Materials Science, University of California, Irvine, Irvine, CA USA 92697-2575

[c]Laser Microbeam and Medical Program, Beckman Laser Institute and Medical Clinic, University of California, Irvine, Irvine, CA USA 92612

[d]National Centre for Biological Sciences, TATA Institute of Fundamental Research, Bangalore, INDIA

[e]Dept. of Chemistry, University of California, Irvine, Irvine, CA

Abstract

Cell lysis and molecular delivery in confluent monolayers of PtK_2 cells are achieved by the delivery of 6 ns, λ = 532 nm laser pulses via a 40×, 0.8 NA microscope objective. With increasing distance from the point of laser focus we find regions of (a) immediate cell lysis; (b) necrotic cells that detach during the fluorescence assays; (c) permeabilized cells sufficient to facilitate the uptake of small (3kDa) FITC-conjugated Dextran molecules in viable cells; and (d) unaffected, viable cells. The spatial extent of cell lysis, cell detachment, and molecular delivery increased with laser pulse energy. Hydrodynamic analysis from time-resolved imaging studies reveal that the maximum wall shear stress associated with the pulsed laser microbeam-induced cavitation bubble expansion governs the location and spatial extent of each of these regions independent of laser pulse energy. Specifically, cells exposed to maximum wall shear stresses $\tau_{w,\,max} > 190 \pm 20$ kPa are immediately lysed while cells exposed to $\tau_{w,\,max} > 18 \pm 2$kPa are necrotic and subsequently detach. Cells exposed to $\tau_{w,\,max}$ in the range 8–18 kPa are viable and successfully optoporated with 3kDa Dextran molecules. Cells exposed to $\tau_{w,\,max} < 8 \pm 1$ kPa remain viable without molecular delivery. These findings provide the first direct correlation between pulsed laser microbeam-induced shear stresses and subsequent cellular outcome.

Keywords

cell viability; membrane permeabilization; molecular delivery; plasma formation; shock wave; cavitation bubble; sonoporation; ultrasonic

1 Introduction

Pulsed laser microbeams offer the ability to deposit energy with high spatial precision to produce controllable perturbations to cellular systems. As a result, there is an increasing interest to use pulsed laser microbeams for precise cellular manipulation, including laser-induced cell lysis [1], cell microdissection and catapulting [2–5], cell collection, expansion,

Address correspondence to: Vasan Venugopalan, Department of Chemical Engineering and Materials Science, 916 Engineering Tower, University of California, Irvine, Irvine, CA 92697-2575, Ph: (949) 824-5802, Fax: (949) 824-2541, vvenugop@uci.edu.

and purification [6–8], cellular microsurgery [9–11], and cell membrane permeabilization for the delivery of membrane-impermeant molecules into cells [12 15], The processes of laser-induced optoinjection and optoporation offer the ability to load cells with a variety of biomolecules on short time scales (milliseconds to seconds) through optically produced cell membrane permeabilization [12, 14, 15], Despite the innovative utilization of laser microbeams in cell biology and biotechnology, only recently have studies provided insight regarding the mechanisms that mediate the interactions of highly focused pulsed laser beams with cells [16–22], A better understanding of these processes will prove critical to the continued development of laser microbeams for both research and practical applications. In previous studies, we provided a detailed characterization of the physics involved in the interaction of highly-focused nanosecond laser microbeams with cells [19, 20], However, it is important to relate these physical effects to the biological response of the cells. The objective of this work is to determine the biological effects resulting from laser-induced cellular injury and connect these effects with the physics of the laser microbeam irradiation process. An understanding of this inter-relationship between the physical processes of pulsed laser microbeam irradiation and the biological response may enable the optimization of the laser parameters used in these procedures and motivate for the development of new applications that utilize laser microbeams.

This study provides a detailed examination of the biophysical effects resulting from pulsed laser microbeam irradiation of a confluent cell monolayer. The irradiation results in laser-induced plasma formation, shock wave propagation, and cavitation bubble formation, expansion, and collapse. These phenomena collectively produce the observed cellular effect. Of particular interest is a hydrodynamic analysis of the cavitation bubble expansion that reveals the effects of fluid shear stress on cell lysis, viability, and transient membrane permeabilization for molecular delivery. We have recently utilized time-resolved imaging methods to show that the cavitation bubble expansion is the primary agent for the lysis of PtK_2 cells when using nanosecond laser microbeams focused at a location 10 μm above the cell monolayer [19, 20], Cell lysis is initiated at the site of plasma formation and propagates outwards with the bubble expansion [20], A hydrodynamic model reveals that for cell monolayers cultured at surface densities of 1000 cells/mm^2, cell lysis occurred only at locations where transient shear stresses $\tau_{w,\,max} > 190 \pm 20$ kPa, independent of the laser pulse energy. Cells exposed to lower shear stresses remained intact and appeared viable even though they were subject to severe transient deformation during the cavitation bubble dynamics. In this study, we investigate the biological response to the delivery of a single pulsed laser microbeam by assessing the cell viability and membrane permeabilization surrounding the site of irradiation as a function of pulse energy. We examine the biophysical implication of these results using quantitative data obtained from time-resolved imaging of the laser microbeam irradiation process and hydrodynamic analysis.

2 Materials and Methods

2.1 Cell Irradiation

An inverted microscope (Axiovert S100, Zeiss, Jena, Germany) was used as the experiment platform. A Q-switched, frequency-doubled Nd:YAG laser (INDI 20, Spectra Physics, Mountain View, CA) emitting 6 ns pulses at $\lambda = 532$ nm was used for cell irradiation. As shown in Figure 1, the laser output was directed through a $\lambda/2$ plate and polarization-sensitive beam splitter, followed by a linear polarizer to adjust the laser pulse energy. The central portion of the laser beam was selected using an iris, directed into the rear microscope port, and reflected upward into the rear entrance aperture of the objective by a dichroic mirror placed in the microscope filter cube. The laser pulse energy entering the rear entrance aperture of the objective was measured by removing the objective from the microscope turret and allowing the unobstructed beam to illuminate an energy detector (Model No.

J5-09, Coherent, Santa Clara, CA) set on the microscope stage. Pulse-to-pulse energy variation was found to be ± 3%. A bright-field objective (40×, 0.8 NA, Achroplan, Zeiss) was used for cell irradiation. The focal plane of the pulsed laser microbeam was positioned at a separation distance of 10 μm above the cell monolayer.

2.2 Fluorescence Imaging

A Quantix CCD camera (Photometries, Roper Scientific, Trenton, NJ) was used to capture fluorescence and phase contrast images with 20×, 0.45 NA Phase 2 (Zeiss A Plan, Jena, Germany) and 10×, 0.3 NA Phase 1 (Zeiss Plan-NEOFLUAR, Jena, Germany) objectives. Camera operation and image acquisition was performed using V++ imaging software (Photometries, Roper Scientific, Trenton, NJ). Image intensity levels were adjusted and images were compiled using Adobe Photoshop 7.0 (Adobe Systems Inc., San Jose, CA).

2.3 PtK_2 Cell Culture

Potorous rat kidney epithelial (PtK_2) cells were grown in polystyrene culture dishes with glass bottoms (P35G-0-14-C, MatTek, Ashland, MA) in advanced minimum essential medium (Advanced MEM, Invitrogen, Carlsbad, CA) supplemented in 1% fetal calf serum, L-glutamine, amphomycin, and gentamicin sulfate. The culture medium was prepared free of phenol red to ensure its transparency to $\lambda = 532$ nm radiation. Cells were cultured in a humidified incubator at a constant temperature of 37°C and 5% CO_2 level. Culture dishes with cells at 100% confluency were used in each experiment. These cells did not exhibit contact inhibition and the surface density (cells/mm^2) was measured and controlled. The results provided are for cell monolayers cultured at a surface density of 1000 cells/mm^2. The cell surface density was determined by counting the number of cells in a square 0.5 mm × 0.5 mm region centered at the site of cell lysis. The site-to-site variation in cell surface density was kept below 10%.

2.4 Cell Viability Assay

Cell viability was assessed using Calcein AM (Invitrogen, Carlsbad, CA), a membrane permeant dye that passes readily through the cell membrane of viable cells and is hydrolyzed by esterases to form fluorescent Calcein that remains inside the cell. Dead cells were identified by Propidium Iodide (Invitrogen, Carlsbad, CA), a DNA intercalating agent that stains the nuclei of dead cells. Cell culture dishes were incubated 30 minutes after laser irradiation and loaded with 2μM Calcein AM and 5μg/mL Propidium Iodide by incubation for 20 min. To remove the remaining dyes, cells were washed carefully with cell culture medium three times before imaging.

2.5 Molecular Delivery Assay

Prior to laser irradiation, cells were placed in a 500μM solution of Fluorescein isothiocyanate (FITC) conjugated Dextran (Sigma, MW=3 kDa). Cells were lysed and incubated for 30 minutes at 37°C, and a 5μg/mL solution of Propidium Iodide (PI) was added. Cells were incubated for an additional 20 min and washed with buffer three times before imaging.

3 Results

3.1 Plasma Threshold, Cell Viability, and Molecular Delivery

The threshold energy for plasma formation in our experimental system is 8μJ [20], This was verified through the delivery of a Nd:YAG laser pulse via the 40×, 0.8 NA bright-field objective into a Petri dish filled with culture medium. Plasma formation in the culture medium was observed visually in a dark room and its incidence for 50 pulses at discrete

pulse energies was recorded. The threshold for plasma formation is defined as the pulse energy that results in a 50% probability of plasma formation.

Cell cultures were irradiated with single laser pulses at energies of 8, 16, 24, and 40 μJ, corresponding to 1×, 2×, 3×, and 5× the threshold energy for plasma formation. A minimum of 10 sites for each pulse energy was examined using fluorescence assays. The extent of cellular damage was confirmed by performing a standard live-dead fluorescence assay using Calcein AM and Propidium Iodide on the cell cultures after irradiation. Immediately after lysis, the irradiation sites were imaged in phase contrast. In addition, we imaged the irradiation sites in both phase contrast and epifluorescence after the cell assays were carried out. In performing the cell assays, we observed that many cells surrounding the lysis zone that remained adherent immediately after laser microbeam irradiation detached and were flushed away during the wash process (Figure 2).

Figure 3 provides phase contrast and epifluorescence images of cells after viability staining for sites irradiated at pulse energies corresponding to 1×, 2×, 3×, and 5× the threshold energy for plasma formation, respectively. The majority of cells that remain attached after the fluorescence assay survive the laser irradiation, as seen by the presence of very few dead cells around laser irradiation site. Outside this region, the cells remain adherent and viable. The area cleared of cells increases with pulse energy. These cells were followed 24 hours post-irradiation to confirm their continued viability, proliferation, and migration to fill in the void areas created by the cell lysis event.

After confirmation that the vast majority of the adherent cells surrounding the irradiation site remain viable, we sought to assess the potential of using pulsed laser microbeam irradiation for molecular delivery. PtK_2 cell cultures were placed in a solution of FITC-conjugated Dextran (MW = 3kDa) and exposed to a single 6 ns pulse from the Nd:YAG laser delivered via the 40×, 0.8 NA bright-field objective. The cells were washed with buffer and dead cells were identified by incubation with Propidium Iodide. Figure 4 shows phase contrast and fluorescent images demonstrating molecular uptake of Dextran after irradiation at all four laser microbeam energies examined. Three zones of cells were identified following molecular delivery. The first region is characterized by necrotic cells that detached during the viability assay. This resulted in only a few remaining adherent cells that showed staining with Propidium Iodide. The second region is occupied by viable cells surrounding the irradiation site in which molecular delivery was achieved as confirmed by uptake of the 3kDa FITC-conjugated Dextran. In the third region, few cells were visibly loaded with the 3kDa FITC-conjugated Dextran; and all of these cells remained viable (as demonstrated in the viability assay shown in Figure 3). Again, the zones of cellular damage and optoporation increase with pulse energy.

3.2 Characterization of the Zones of Cellular Injury

Collectively, the assays that evaluated the cellular response to laser-generated cavitation bubbles revealed four distinct zones of cellular injury. Previously, we identified the radius of cell lysis R_{lys} as the radius of the region around the irradiation site that was denuded of cells immediately after laser irradiation [20], Upon completion of the viability and membrane permeability assays, we found many cells beyond this region to be necrotic and, as mentioned previously and shown in Figure 2, detach during the wash process associated with the cell assays. Moreover, a few cells that remained adherent were also necrotic. Therefore, we have defined a second radial location, $r = R_{necr}$, that denotes the maximum radius at which cell necrosis is seen and beyond which cells remain adherent and viable. Beyond this region, we have identified a third radial location $r = R_{perm}$ that characterizes the spatial extent of permeabilized cells i.e., cells that display uptake of the 3kDa FITC-Dextran following laser irradiation as viewed through standard fluorescence microscopy. Beyond

R_{perm} the cells are viable, show no uptake of the 3kDa FITC-conjugated Dextran and appear to be unaffected by the laser microbeam irradiation. A schematic illustrating these regions is shown in Figure 5.

The average and standard deviation of the locations of each of these zones were determined by measuring the radius of cellular injury produced at 8–10 irradiation sites. In some instances the zone of cell lysis was slightly elliptical and the radius of a circle of equivalent area was used instead. The radial dimension defining the zones of cellular injury as a function of pulse energy is shown in Table 1. As reported previously, we found the radius of cell lysis, R_{lys}, to be 23, 30, 36, and 56μm for pulse energies corresponding to 1×, 2×, 3×, and 5× threshold, respectively [20], The viability assays revealed values of R_{necr} to be 66, 105, 134, and 165μm for pulse energies corresponding to 1×, 2×, 3×, and 5× threshold, respectively. The maximum radial location occupied by permeabilized cells, R_{perm}, were measured as 101, 162, 202, and 252μm for pulse energies corresponding to 1×, 2×, 3×, and 5× threshold, respectively. In Table 1 we also provide an estimate for the number of optoporated cells by taking the product of the area of cell permeabilization and the cell surface density of 1000 cells/mm^2. Collectively, the results demonstrate that increases in pulse energy produce substantial increases in both the zones of cellular damage and the number of permeabilized cells.

4 Analysis and Discussion

Our rich data set provides the opportunity to examine the experimental observations with respect to those of other investigators and to explore the possible connection between the zones of cell lysis, necrosis, and cell membrane permeabilization with the underlying physical mechanisms. From the mechanistic standpoint, we will examine the potential contributions of cavitation bubble-induced shear stress and shock wave pressure to cell lysis and cell membrane permeabilization. This is achieved through hydrodynamic modeling facilitated by a quantitative assessment of time-resolved images of the cavitation bubble expansion generated by the delivery of pulsed laser microbeam irradiation to confluent PtK_2 cell cultures at the same pulse energies examined in the cellular assays. Finally, we discuss our laser-based molecular delivery results for relative to those of other studies as well as studies in acoustic cavitation literature that examine sonoporation as a means for molecular delivery.

4.1 Role of Cavitation Bubble Generated Shear Stress on Cell Lysis and Membrane Permeabilization

Our previous time-resolved imaging study of the pulsed laser microbeam cell lysis process provided evidence that the primary agent for cell lysis and deformation is the dynamic shear stress produced by the cavitation bubble expansion [20], We introduced a hydrodynamic model to determine the spatio-temporal evolution of both the fluid velocity and wall shear stress provided by the cavitation bubble dynamics. This model revealed a direct relationship between the maximum wall shear stress $\tau_{w,\,max}$ and the extent of cell lysis R_{lys}. A schematic of this model is shown in Figure 6a. In this model we assume that the cell monolayer acts as a stationary boundary and that the cells are subject to shear stress due to movement of fluid parallel to this boundary. We consider the fluid motion at locations outside the expanding bubble and define a geometry in which the origin is located at the site of the laser focus immediately above the cell monolayer with z and r being the vertical and radial axes, respectively.

Time-resolved imaging provided a means to quantify the spatial and temporal evolution of both the radial position $R_B(t)$ and velocity $V_B(t)$ of the bubble wall. A sample set of this data

is shown in Figure 6b. Conservation of mass in this system provides the following relationship between the external fluid velocity $V_\infty(r, t)$ and the bubble dynamics as:

$$V_\infty(r,t)=V_B(t)\left[\frac{R_B(t)}{r}\right]^2, \tag{1}$$

Conservation of momentum was then applied to obtain the following expression for the wall shear stress $\tau_w(r, t)$ generated by the cavitation bubble expansion [20]:

$$\tau_w(r,t)=\rho\sqrt{\frac{\nu}{\pi}}\int_0^t\frac{\partial V_\infty(r,t')}{\partial t'}\frac{dt'}{\sqrt{t-t'}} \tag{2}$$

where ρ and ν are is the density and kinematic viscosity of the fluid medium [20], Equation (2) is valid at any radial position r and time $0 \le t \le t'$ where t' is the time of arrival of the bubble wall at position r.

The profiles of the temporal evolution of the wall shear stress are characterized generally by a rapid ($\lesssim$ 30 ns) increase to a maximum value followed by a more gradual decay [20], Of particular interest is the maximum shear stress at radial positions corresponding to the regions of cell lysis, cell necrosis, and cell membrane permeabilization. In Table 2 we provide the maximum wall shear stress predicted by our hydrodynamic analysis at each of these interfaces as described in the Results i.e., at $r = R_{lys}$, $r = R_{necr}$, and $r = R_{perm.}$ This table encompasses pulse energies in the range 8–40μJ, corresponding to energies of 1×–5× the threshold for plasma formation. Remarkably, even with wide range of pulse energies examined, the range of shear stresses calculated at each zone of cellular injury is quite narrow; typically $\lesssim$ 10%. The location representing the maximum extent of immediate cell lysis ($r = R_{lys}$) is exposed to maximum wall shear stresses of $\tau_{w,\,max} = 190 \pm 20$ kPa, whereas the location representing the maximum extent of necrotic cells ($r = R_{necr}$) is exposed to shear stresses $\tau_{w,\,max} = 18 \pm 2$ kPa. Finally the analysis indicates that the molecular delivery to these cells with a 3kDa FITC-conjugated Dextran through transient membrane permeabilization ($r = R_{perm}$). requires a maximum transient shear stress of $\tau_{w,\,max} = 8 \pm 1$ kPa. Cells exposed to $\tau_{w,\,max} \lesssim 8 \pm 1$ kPa remain viable and appear unaffected by the pulsed laser microbeam irradiation.

Figure 7 illustrates the interrelationship between the spatial region occupied by the lysed, necrotic, optoporated, and unaffected cells and the maximum transient shear stress for all 4 pulse energies tested. The curves represent the predictions of the hydrodynamic model for the maximum wall shear stress as a function of radial position for each laser microbeam pulse energy. The shaded regions are defined by the range of shear stresses necessary for the pulsed laser microbeam to produce the appropriate cellular effect. The intersection of an individual curve with each shaded region defines the range of maximum wall shear stress and radial positions in which the various cellular effects are achieved for the given pulse energy. The mean and standard deviation of the experimental results for R_{lys}, R_{necr}, and R_{perm} and the corresponding $\tau_{w,\,max}$ predicted by the hydrodynamic model at these locations are also shown. The location of the experimental data points across all pulse energies is remarkably consistent with the boundaries of the shaded regions.

The collective congruence between the experimental results and hydrodynamic modeling identifies a well-defined range of maximum transient wall shear stress of 8–18 kPa required to achieve molecular delivery while maintaining cell viability of 3kDa FITC-conjugated Dextran for PtK_2 cells cultured at a density of 1000 cells/mm^2. Transient wall shear stresses

below 8kPa do not achieve optoporation, while transient wall shear stresses above 18kPa result in loss of cell viability through cell necrosis and detachment and, for $\tau_{w,\,max} > 190$ kPa, through immediate cell lysis. It is important to emphasize that previous experiments have shown that the maximum shear stresses necessary to produce cell lysis decreases with a reduction in the cell surface density [20], Thus it is expected that cell surface densities < 1000 cells/mm^2 will result in a lower range of shear stresses to produce optoporation. Moreover, we expect that the specific values of the maximum transient wall shear stress necessary to achieve the observed cellular effects will change with cell type.

4.2 Potential Role of Shock/Stress Waves to Achieve Molecular Delivery

Thus far, we have not considered the potential contribution of the shock wave produced by plasma formation to the observed cellular effects. Our previous studies [19, 20] have provided no evidence for the role of shock waves in the production of the observed cellular effects. Rather, these studies have implicated the cavitation bubble dynamics as the primary instigator of cellular damage and cell membrane permeabilization. Nevertheless, there have been extensive studies investigating the specific contribution of laser-generated stress/shock waves to cellular injury as well as molecular delivery [23 28], The study most relevant to our investigation is that of Kodama and co-workers who investigated the efficacy of laser-generated and shock tube-generated pressure waves to produce molecular delivery of Calcein (MW=622 Da) and FITC-conjugated Dextran (MW=71.4kDa) into the cytoplasm of HL-60 human promyelocytic leukemia cells. They found that the efficacy of molecular delivery was not correlated with the maximum shock wave pressure but rather with the shock wave impulse as estimated by the product of the maximum pressure and the shock duration. They found that to achieve molecular delivery to roughly 45% of the cells requires an impulse of ~ 50 Pa·s for Calcein and ~ 150 Pa·s for the 71.4 kDa FITC-conjugated Dextran.

We have measured velocity of the shock waves produced by pulsed laser microbeam irradiation as a function of both pulse energy and radial position to determine the shock wave pressure [19], This analysis reveals that the cells which are successfully optoporated receive maximum shock pressures not exceeding 50 MPa [19] and that these shock waves possess a characteristic duration of 40 ns [18], This results in a maximum impulse of 2 Pa·s; 25× below the impulse required to achieve molecular delivery as reported by Kodama and co-workers. We thus conclude that the shock wave generated by the pulsed laser microbeam irradiation is unlikely to provide a contribution to the observed molecular delivery of 3 kDa FITC-conjugated Dextran in our system. Nevertheless, there may be similarities in the underlying mechanism by which shock waves and transient fluid shear stress causes structural changes in the cell membrane to facilitate molecular delivery. Such structural changes in the phospholipid bilayer have been recently investigated via molecular dynamics simulations by Koshiyama and co-workers for the case of shock wave-generated molecular delivery [28], Clearly the use of such computational methods to examine the impact of transient fluid shear stress on the structure of the phospholipid bilayer would represent an important next step to elucidate the molecular mechanisms of this process.

4.3 Implications for Molecular Delivery and Acoustic Cavitation Studies

The characteristics of our molecular delivery results are similar to those reported by Soughayer and co-workers who investigated the molecular delivery of rat basophilic leukemia (RBL) cells using a single 5 ns, $\lambda = 532$ nm laser pulse with 10μJ pulse energy delivered via a 100×, 1.3 NA microscope objective [14], The RBL cells were placed in a 170μM solution of 3 kDa Texas Red-conjugated Dextran. Soughayer and co-workers identified three distinct zones of cellular response following the pulsed laser microbeam irradiation: (a) a region of dead and/or detached cells at distances of up to 30μm from the

laser irradiation site, (b) a region of optoporated, viable cells 31–60μm from the irradiation site, and (c) seemingly unaffected, viable cells that showed little uptake of the Texas Red-conjugated Dextran at distances > 60 μm from the irradiation site. Differences between the spatial extent of the three zones of cellular effects between the two studies are likely due to the different cell types, cell surface density, and microscope objective. Our results for 8μJ pulse energy (1× threshold), provides a similar ~30μm range for immediately lysed cells and a similar ~30μm wide region of permeabilized cells.

Also of interest is a comparison of our results with the use of cavitation bubbles created by acoustic means for applications in cell lysis, cell detachment, and molecular delivery [13, 16, 19, 20, 29], Recently, much attention has been given to the use of ultrasonic techniques to achieve molecular delivery to cells and tissues for therapeutic applications such as transdermal drug delivery, gene therapy, and delivery of chemotherapeutic drugs to tumors [30], The use of low-amplitude ultrasound to achieve transient cell membrane permeabilization for molecular delivery is known as reparable sonoporation [31]. It has been found that sonoporation is enhanced significantly when cavitation bubbles are present during the acoustic exposure, suggesting that a fluid dynamic interaction between cavitation bubbles and cells is responsible for membrane poration [17, 31, 32], The physical mechanism of sonoporation is not well understood and thus the dependence of membrane permeabilization on the cavitation parameters is not yet known [33, 34], A better understanding of the physical mechanisms responsible for the poration of the cell membrane is crucial for the optimization of this technique. As a result many groups are examining ultrasound-generated cavitation bubble dynamics and the resulting fluid velocities to determine the shear stresses and exposure times required to achieve sonoporation, cell detachment, and cell lysis [16, 17, 29, 35, 36].

Wu and co-workers have examined acoustic cavitation by subjecting an erythrocyte suspension to an oscillating probe called a Mason horn set to a frequency of 20 kHz, a technique referred to as microstreaming [29, 35], They developed a mathematical model to estimate the shear stress experienced by Jurkat leukocytes subject to microstreaming and concluded that the shear stress produced by the Mason horn was the primary mechanism for the cells demonstrating reparable sonoporation. This study determined that a threshold shear stress of 12 ± 4 Pa is required for reparable sonoporation for exposures of up to 7 minutes [29, 35], Similar studies using microstreaming have also determined shear stress to be the mechanism of hemolysis of erythrocytes, with a critical shear stress for hemoglobin release was found to be in the range of 300–450 Pa [35, 37], Threshold shear stresses have not been determined for all cell types, but it has been shown that lysis of red blood cells by local shear has a strong dependence on cell volume [38, 39], Extrapolation of these data to endothelial cells predicts lysis to occur at stresses of ~ 800 Pa [40], Studies by Ohl and Wolfrum found a 100–160 Pa shear stress required for detachment of cultured HeLa cells using a lithotripter [16], and reparable sonoporation was observed at shear stresses below the 100 Pa required for cell detachment. In all of these studies, the reported shear stress values for molecular delivery and cell lysis are on the order of 100 Pa for exposure times on the order of minutes. By contrast, the shear stress values required for cell lysis and molecular delivery using pulsed laser microbeams are in the 10–100 kPa regime; stress magnitudes that are larger by two to three orders of magnitude. However, the duration of these stress transients are on the order of nanoseconds to microseconds. This suggests strongly that there exists a time-stress dependent mechanism for stress-mediated permeabilization and damage to the cell membrane.

The use of sonoporation for molecular delivery to cells and tissues holds promise for many therapeutic applications in the medicine. However, typical sonoporation experiments result in the production of multiple cavitation bubbles whose exact size and location are not

controlled. The use of pulsed laser microbeams offers the advantage of creating individual cavitation bubbles of specific size and location. This enables the generation of controlled and reproducible regions of cellular damage and/or molecular delivery. Moreover, with the potential development of laser microbeam platforms that offer multiple wavelengths (e.g., λ = 355,532,1064nm) and a range of pulse durations (ns-fs) that can provide for optical breakdown over a range of pulse energies [41, 22], one can easily conceive of a single platform that can provide for precise zones of cellular damage and molecular delivery over a broad range.

5 Conclusion

We have examined the cellular response of adherent PtK_2 cell monolayer to nanosecond pulsed laser microbeam irradiation. Cell viability and membrane permeability assays combined with microscopic examination have identified and quantified regions of (a) immediate cell lysis, (b) cell necrosis, and (c) molecular delivery in response to 6 ns pulsed laser microbeam irradiation at λ = 532 nm in cell monolayers cultured at a density of 1000cells/mm^2. Hydrodynamic analysis of the cavitation bubble dynamics produced by the laser microbeam irradiation revealed that over a 5-fold variation in laser microbeam energy, the spatial extent of each of these regions are linked to the maximum transient shear stress produced by the fluid displaced by the cavitation bubble expansion. Specifically, for cells immediately adjacent to the site of irradiation that experienced maximum transient wall shear stresses $\tau_{w.max} > 190 \pm 20$kPa, were immediately lysed. Cells that were situated further away that were exposed to $\tau_{w.max} > 19 \pm 2$ kPa remained intact but were necrotic. Cells positioned more distant that received maximum shear stresses in the range $8 \pm 1 \leq \tau_{w.max} \leq 19 \pm 2$ kPa remained viable and were successfully optoporated with 3kDa FITC-conjugated Dextran molecules. At all pulse energies, cells were transiently permeabilized up to 2 to 3 layers around the lysis zone, indicating that this range of transient shear stress produces a transient, but repairable, disruption in the plasma cell membrane. Finally, cells most distant from the irradiation site that received $\tau_{w.max} < 8 \pm 1$ kPa remained intact, viable and free of molecular delivery.

Of interest is the fact that the ranges of maximum shear stresses necessary to produce cell lysis, necrosis and molecular delivery using laser microbeams are of the order of 10–100kPa; roughly 3 orders of magnitude larger than those typically utilized for cell lysis and molecular delivery by the ultrasonic/sonoporation community. The important difference is that the exposure to these stresses are typically of the order of 0.1–10 μs when using pulsed laser microbeam irradiation and 1–100 seconds when using ultrasonic sources. This strongly suggests a stress-time dependent mechanism for mechanical damage of the cell membrane that warrants further examination.

This study has identified a well-defined range of maximum wall shear stress (~8–18kPa) required to achieve molecular delivery through optoporation. Through investigation of the damage zones and resulting shear stress caused by cavitation bubble expansion, this technique can be used to optimize optoporation of diverse molecules into varying cell types. In contrast to sonoporation, the use of pulsed laser microbeams offer the advantage of producing cavitation bubbles with reproducible size and specific location that, in turn, can produced well-defined, reproducible zones of cell lysis, optoporation, and cell viability.

Acknowledgments

We thank Carole Hayakawa for computational assistance. We acknowledge support from the National Institutes of Health via the Laser Microbeam and Medical Program P41-RR-01192 and R01-EB04436. Support has also been provided by the University of California Systemwide Biotechnology Research and Education Program GREAT Training Grant, # 2006-12.

References

1. Sims CE, Meredith GD, Krasieva TB, Berns MW, Tromberg BJ, Allbritton NL. Laser-micropipet combination for single cell analysis. Analytical Chemistry. 1998; 70(21):4570–4577. [PubMed: 9823716]
2. Schütze K, Becker I, Becker KF, Thalhammer S, Stark R, Heckl WM, Böhm M, Pösl H. Cut out or poke in – the key to the world of single genes: laser micromanipulation as a valuable tool on the look-out for the origin of disease. Genetic Analysis and Biomolecular Engineering. 1997; 14:1–8.
3. Schütze K, Pösl H, Lahr G. Laser micromanipulation systems as universal tools in cellular and molecular biology and in medicine. Cell and Molecular Biology. 1998; 44(5):735–746.
4. Schütze K, Lahr G. Identification of expressed genes by laser-mediated manipulation of single cells. Nature Biotechnology. 1998; 16(8):737–742.
5. Vogel A, Horneffer V, Lorenz K, Linz N, Hüttmann G, Gebert A. Principles of laser microdissection and catapulting of histologic specimens and live cells. Methods in Cell Biology. 2007; 82:153–205. [PubMed: 17586257]
6. Palsson, BO.; Koller, MR.; Eisfeld, TM. Method and apparatus for selectively targeting specific cells within a mixed cell population. United States Patent. 6534308B1. March. 2003
7. Salazar GT, Wang Y, Young G, Bachman M, Sims CE, Li GP, Allbritton NL. Micropallet arrays for the separation of single, adherent cells. Analytical Chemistry. 2007; 79(2):682–687. [PubMed: 17222037]
8. Wang Y, Young G, Bachman M, Sims CE, Li GP, Allbritton NL. Collection and expansion of single cells and colonies released from a micropalet array. Analytical Chemistry. 2007; 79(6):2359–2366. [PubMed: 17288466]
9. Berns MW, Aist J, Edwards J, Strahs K, Girton J, McNeill P, Rattner JB, Kitzes M, Hammer-Wilson M, Liaw LH, Siemens A, Koonce M, Peterson S, Brenner S, Burt J, Walter R, Bryant PJ, van Dyk D, Coulombe J, Cahill T, Berns GS. Laser microsurgery in cell and developmental biology. Science. 1981; 213:505–513. [PubMed: 7017933]
10. Berns MW, Wang Z, Dunn A, Wallace V, Venugopalan V. Gene inactivation by multiphoton-targeted photochemistry. Proceedings of the National Academy of Sciences USA. 2000; 97:9504–9507.
11. Hutson MS, Tokutake Y, Chang MS, Bloor JW, Venakides S, Kiehart DP, Edwards GS. Forces for morphogenesis investigated with laser microsurgery and quantitative modeling. Science. 2003; 300(5616):145–149. [PubMed: 12574496]
12. Tao W, Wilkinson J, Stanbridge EJ, Berns MW. Direct gene transfer into human cultured cells facilitated by laser micropuncture of the cell membrane. Proceedings of the National Academy of Sciences USA. 1987; 84:4180–4184.
13. Krasieva TB, Chapman CF, Lamorte VJ, Venugopalan V, Berns MW, Tromberg BJ. Cell permeabilization and molecular transport by laser microirradiation. Proceedings of the SPIE. 1998; 3260:38–44.
14. Soughayer JE, Krasieva TB, Jacobson SC, Ramsey JM, Tromberg BJ, Allbritton NL. Characterization of cellular optoporation with distance. Analytical Chemistry. 2000; 72(6):1342–1347. [PubMed: 10740880]
15. Clark IB, Hanania EG, Stevens J, Gallina M, Fieck A, Brandes R, Palsson BO, Koller MR. Optoinjection for efficient targeted delivery of a broad range of compounds and macromolecules into diverse cell types. Journal of Biomedical Optics. 2006; 11(1):014034. (8 pages). [PubMed: 16526911]
16. Ohl CD, Wolfrum B. Detachment and sonoporation of adherent HeLa-cells by shock wave-induced cavitation. Biochimica Biophysica Acta. 2003; 1624:131–138.
17. Ohl CD, Arora M, Ikink R, de Jong N, Versluis M, Delius M, Lohse D. Sonoporation from jetting cavitation bubbles. Biophysical Journal. 2006; 91(11):4285–4295. [PubMed: 16950843]
18. Venugopalan V, Guerra A III, Nahen K, Vogel A. Role of laser-induced plasma formation in pulsed cellular microsurgery and micromanipulation. Physical Review Letters. 2002; 88(7): 078103. (4 pages). [PubMed: 11863944]

19. Rau KR, Guerra AG III, Vogel A, Venugopalan V. Investigation of laser-induced cell lysis using time-resolved imaging. Applied Physics Letters. 2004; 84:2940–2942.
20. Rau KR, Quinto-Su PA, Hellman AN, Venugopalan V. Pulsed laser microbeam-induced cell lysis: Time-resolved imaging and analysis of hydrodynamic effects. Biophysical Journal. 2006; 91(1): 317–329. [PubMed: 16617076]
21. Quinto-Su PA, Venugopalan V. Mechanisms of laser cellular microsurgery. Methods in Cell Biology. 2007; 82:113–151. [PubMed: 17586256]
22. Vogel A, Noack J, Huttman G, Paltauf G. Mechanisms of femtosecond laser nanosurgery of cells and tissues. Applied Physics B. 2005; 81:1015–1047.
23. Doukas AG, McAuliffe DJ, Lee S, Venugopalan V, Flotte TJ. Physical factors involved in stress-wave-induced cell injury: The effect of stress gradient. Ultrasound in Medicine and Biology. 1995; 21(7):961–967. [PubMed: 7491750]
24. Lee ST, Anderson T, Zhang H, Flotte TJ, Doukas AG. Alteration of cell membrane by stress waves in vitro. Ultrasound in Medicine and Biology. 1996; 22(9):1285–1293. [PubMed: 9123654]
25. Lee S, Doukas AG. Laser generated stress waves and their effects on the cell membrane. IEEE Journal of Selected Topics in Quantum Electronics. 1999; 5(4):997–1003.
26. Kodama T, Hamblin MR, Doukas AG. Cytoplasmic molecular delivery with shock waves; Importance of impulse. Biophysical Journal. 2000; 79(4):1821–1832. [PubMed: 11023888]
27. Kodama T, Doukas AG, Hamblin MR. Shock wave-mediated molecular delivery into cells. Biochimica et Biophysica Acta – Molecular Cell Research. 2002; 1542:186–194.
28. Koshiyama K, Kodama T, Yano T, Fujikawa S. Structural change in lipid bilayers and water penetration induced by shock waves: Molecular dynamics simulations. Biophysical Journal. 2006; 91(3):2198–2205. [PubMed: 16798798]
29. Wu JR. Shear stress in cells generated by ultrasound. Progress in Biophysics & Molecular Biology. 2007; 93(1–3):363–373. [PubMed: 16928394]
30. Mitragotri S. Innovation - healing sound: the use of ultrasound in drug delivery and other therapeutic applications. Nature Reviews Drug Discovery. 2005; 4(3):255–260.
31. Ward M, Wu JR, Chiu JF. Ultrasound-induced cell lysis and sonoporation enhanced by contrast agents. Journal of the Acoustical Society of America. 1999; 105(5):2951–2957. [PubMed: 10335644]
32. Bao SP, Thrall BD, Miller DL. Transfection of a reporter plasmid into cultured cells by sonoporation in vitro. Ultrasound in Medicine and Biology. 1997; 23(6):953–959. [PubMed: 9300999]
33. Miller MW, Miller DL, Brayman AA. A review of in vitro bioeffects of inertial ultrasonic cavitation from a mechanistic perspective. Ultrasound in Medicine and Biology. 1996; 22(9): 1131–1154. [PubMed: 9123638]
34. Sundaram J, Mellein BR, Mitragotri S. An experimental and theoretical analysis of ultrasound-induced permeabilization of cell membranes. Biophysical Journal. 2003; 84(5):3087–3101. [PubMed: 12719239]
35. Wu JR, Ross JP, Chiu JF. Reparable sonoporation generated by microstreaming. Journal of the Acoustical Society of America. 2002; 111(3):1460–1464. [PubMed: 11931323]
36. Junge L, Ohl CD, Wolfrum B, Arora M, Ikink R. Cell detachment method using shock-wave-induced cavitation. Ultrasound in Medicine and Biology. 2003; 29(12):1769–1776. [PubMed: 14698344]
37. Williams AR, Hughes DE, Nyborg WL. Hemolysis near a transversely oscillating wire. Science. 1970; 169(3948):871. [PubMed: 17750061]
38. Miller MW. Cell size relations for sonolysis. Ultrasound in Medicine and Biology. 2004; 30(10): 1263–1267. [PubMed: 15582225]
39. Miller MW, Sherman TA, Brayman AA. Comparative sensitivity of human and bovine erythrocytes to sonolysis by 1-MHz ultrasound. Ultrasound in Medicine and Biology. 2000; 26(8): 1317–1326. [PubMed: 11120370]
40. VanBavel E. Effects of shear stress on endothelial cells: Possible relevance for ultrasound applications. Progress in Biophysics & Molecular Biology. 2007; 93(1–3):374–383. [PubMed: 16970981]

41. Vogel A, Venugopalan V. Mechanisms of pulsed laser ablation of biological tissues. Chemical Reviews. 2003; 103(2):577–644. [PubMed: 12580643]

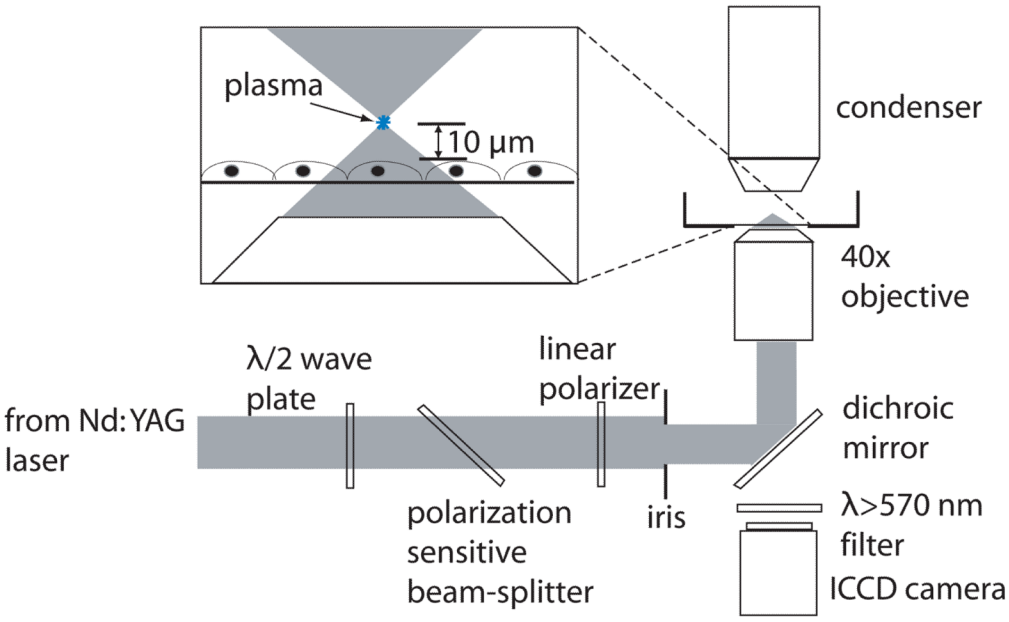

Figure 1.
Schematic of laser-microscope setup for cell lysis.

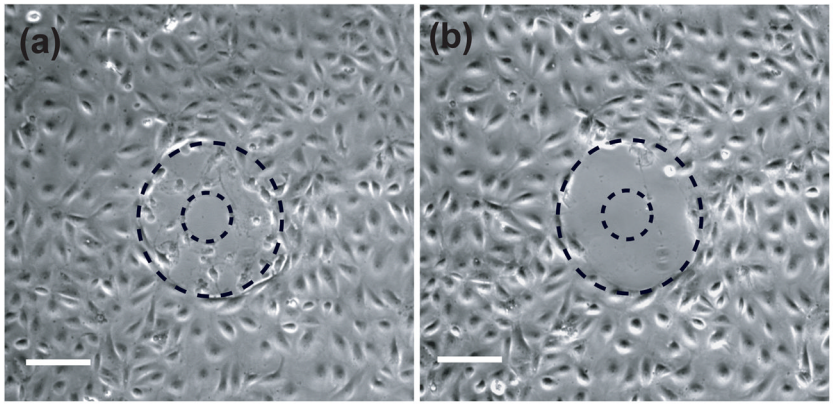

Figure 2.
Phase contrast images of cells following irradiation by a 16μJ laser pulse (2× threshold). Images were taken (a) immediately after lysis and (b) after the viability assay incubation and wash process. Scale bar = 100μm.

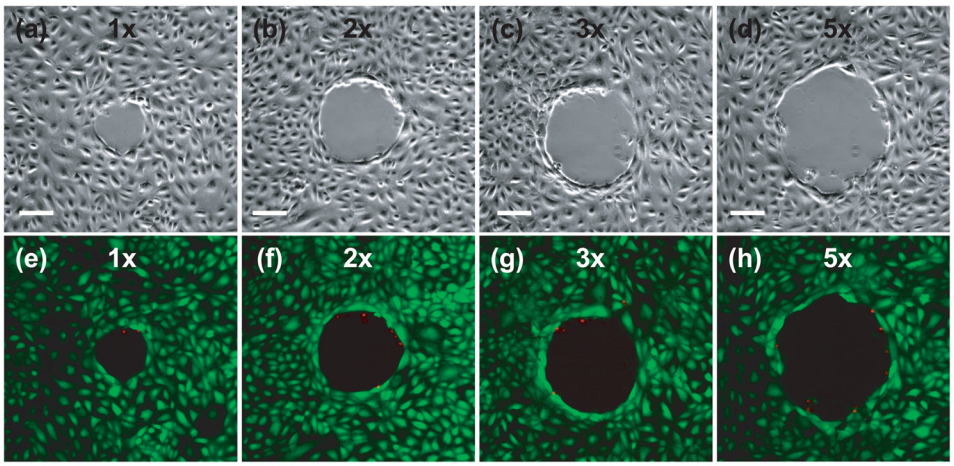

Figure 3.
Cell viability assay after irradiation at energies corresponding to 1× (a,e), 2× (b,f), 3× (c, g) and 5× (d, h) the threshold energy for plasma formation: (a–d) phase contrast images showing the irradiation site and zone of cellular damage (R_{necr}), (e–h) fluorescent images with Calcein AM (green) showing viable cells and Propidium Iodide (red) staining the nuclei of dead cells around the periphery of the irradiation site. Scale bar = 100 μm.

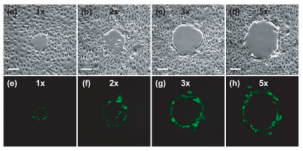

Figure 4.
Membrane permeabilization after irradiation at energies corresponding to 1× (a,e), 2× (b,f), 3× (c, g) and 5× (d, h) the threshold energy for plasma formation: (a–d) phase contrast image showing the irradiation site and damage zone, (e–d) fluorescent image showing cells loaded with FITC-Dextran (green) and Propidium Iodide (red) staining the nuclei of dead cells around the periphery of the irradiation site. Scale bar = 100 μm.

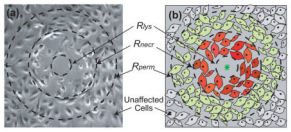

Figure 5.

Zones of cellular injury. We provide a phase contrast image (a) and a schematic drawing (b) illustrating the three measured zones of cellular injury. Some of the cells outside of the lysis zone, R_{lys}, have lost viability and wash away during the assay wash process, creating another damage zone, R_{necr}, beyond which cells remain viable. Beyond this region, we have cells that remained viable and showed molecular uptake of the 3kDa FITC-conjugated Dextran, R_{perm}, beyond which the cells to not appear to be affected by the laser irradiation.

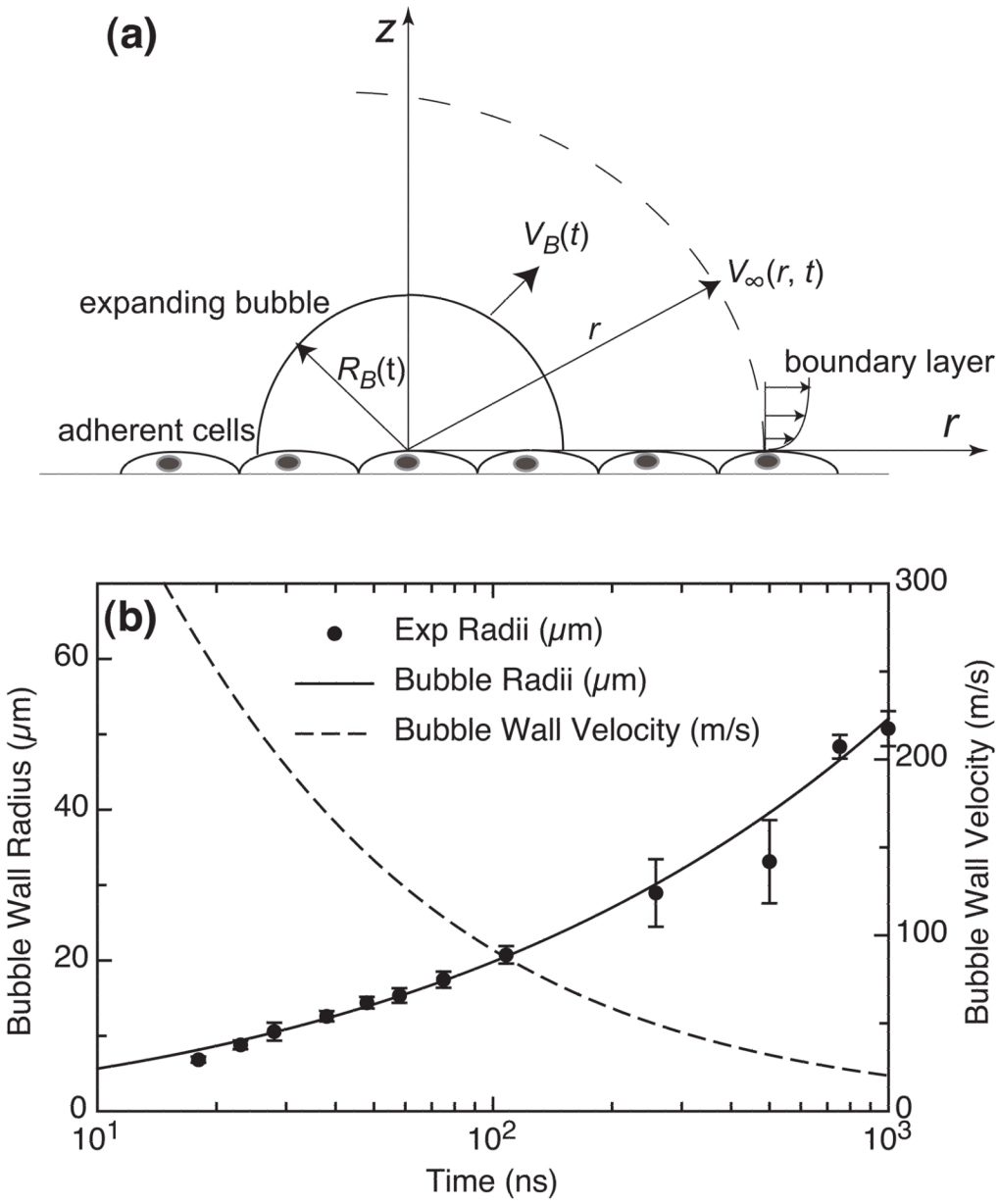

Figure 6.

(a) Schematic of model problem for hydrodynamic analysis. Figure not to scale, (b) Time evolution of the cavitation bubble wall position $R_B(t)$ and velocity $V_B(t)$ determined from time- resolved images of the laser microbeam irradiation event at a pulse energy corresponding to 1× the threshold for plasma formation [20].

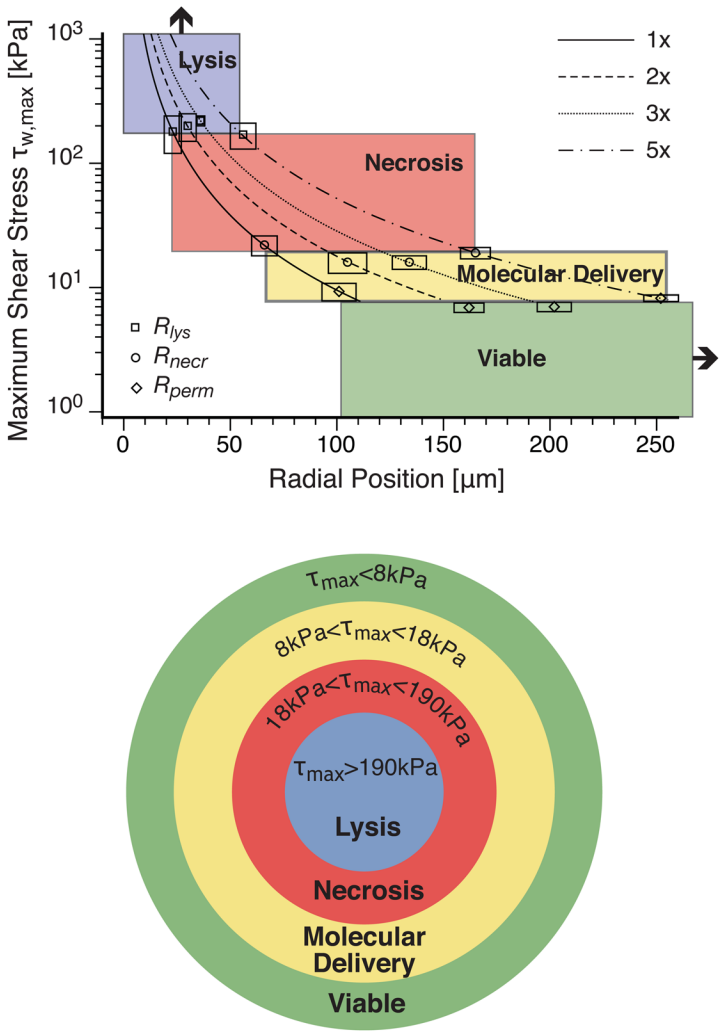

Figure 7.

Composite diagram showing hydrodynamic model predictions of the maximum wall shear stress $\tau_{w,\,max}$ as a function of radial position at pulse energies 1×, 2×, 3×, and 5× the threshold for plasma formation. Colored regions indicate the resulting cellular effect. Experimental data points including error bars validate the hypothesis that the specific ranges of maximum shear stress effectively delimit the separation between regions. These shear stress regions and corresponding cellular effect are depicted pictorially below the main plot.

Table 1

Laser pulse energy (E_p), radius of cell lysis (R_{lys}), radius of cell necrosis (R_{necr}), radius of permeabilized cells (R_{perm}), and the number of permeabilized cells when irradiating cell cultures with a cell surface density of 1000 cells/mm^2 at pulse energies corresponding to 1×, 2×, 3×, and 5× the threshold for plasma formation.

	E_P[μJ]	R_{lys} [μm]	R_{necr} [μm]	R_{perm} [μm]	# Permeabilized Cells
1× Threshold	8	23 ± 4	66 ± 6	101 ± 8	18 ± 6
2× Threshold	16	30 ± 4	105 ± 9	162 ± 7	48 ± 9
3× Threshold	24	36 ± 2	134 ± 8	202 ± 8	72 ± 12
5× Threshold	40	56 ± 6	165 ± 7	252 ± 8	114 ± 13

Table 2

Summary of hydrodynamic data and analysis providing the maximum wall shear stress $\tau_{w,\,max}$ computed at each zone of cellular injury for pulse energies corresponding to 1×, 2×, 3×, and 5× the threshold for plasma formation.

		Maximum wall shear stress $\tau_{w,\,max}$ [kPa]		
	E_P [μJ]	$r = R_{lys}$	$r = R_{necr}$	$r = R_{perm}$
1× Threshold	8	180 ± 60	22 ± 4	9.3 ± 1.5
2× Threshold	16	200 ± 50	16 ± 3	6.9 ± 0.6
3× Threshold	24	220 ± 20	16 ± 2	7.0 ± 0.6
5× Threshold	40	170 ± 40	19 ± 2	8.2 ± 0.5
Mean±SD		190 ± 20	18 ± 2	8.0 ± 1.0